Title	Bandwidth Enhancement of Doherty Power Amplifier Using Modified Load Modulation Network
Authors(s)	Li, Meng; Pang, Jingzhou; Li, Yue; Zhu, Anding
Publication date	2020-06
Publication information	IEEE Transactions on Circuits and Systems I: Regular Papers, 67 (6): 1824-1834
Publisher	IEEE
Item record/more information	http://hdl.handle.net/10197/11746
Publisher's statement	© 2020 IEEE. Personal use of this material is permitted. Permission from IEEE must be obtained for all other uses, in any current or future media, including reprinting/republishing this material for advertising or promotional purposes, creating new collective works, for resale or redistribution to servers or lists, or reuse of any copyrighted component of this work in other works.
Publisher's version (DOI)	10.1109/tcsi.2020.2972163

Bandwidth Enhancement of Doherty Power Amplifier Using Modified Load Modulation Network

Meng Li, *Student Member, IEEE,* Jingzhou Pang, *Member, IEEE,* Yue Li, *Student Member, IEEE,* and Anding Zhu, *Senior Member, IEEE*

***Abstract*—A novel Doherty power amplifier (DPA) architecture with extended bandwidth is presented in this paper. A modified load modulation network is introduced to provide impedance condition required by the Doherty operation in a wide frequency range. Analytical parameter solutions of the proposed load modulation network and the related load modulation process are presented. A DPA with 2.80-3.55 GHz bandwidth utilizing commercial GaN transistors is implemented. The fabricated DPA attains a measured 9.3-11.1 gain and 43.0-45.0 dBm saturated power. 50.0-60.6% and 66-78% drain efficiency is obtained at 6 dB output power back-off and saturation throughout the designed band, respectively. Moreover, the back-off drain efficiencies are higher than 55% within 700 MHz bandwidth. When driven by a 6-carrier 120 MHz OFDM signal with 7.0 dB peak to average power ratio, the proposed DPA achieves adjacent channel leakage ratio of better than -50 dBc after digital pre-distortion (DPD) at 3.20 GHz with average efficiency of 53.3%.**

***Index Terms*—broadband, Doherty power amplifier, high efficiency, load modulation**

I. Introduction

TO improve spectrum efficiency, modulated non-constant envelope signals with high peak to average power ratio (PAPR) have been widely adopted in modern wireless communication systems. Since the radio frequency (RF) power amplifier (PA) is the most power consuming component in wireless transmitters and the system efficiency relies on the average power efficiency, it is thus crucial to maintain high efficiency performance of the PA at the output power back-off (OBO) [1]–[4]. Several PA architectures have been proposed to improve back-off efficiency, such as, Doherty power amplifier (DPA), envelope tracking (ET), out-phasing and many others. Among them, the DPA is one of the most popular PA architectures deployed in cellular base stations due to its high reliability and simple circuit structure [5]–[8].

Meanwhile, with the rapid development of wireless communication standards, more and more frequency bands have been added in wireless communication systems [9]. The increasing number of the operation frequency bands creates strong demands for bandwidth extension techniques of PAs. With the advent of the 5G era, this demand is even more urgent since the 5G air-interface will adopt more new frequency bands and the bandwidth of the transmit signals will also become much wider. In response to this demand, a lot of efforts have been made in extending the bandwidth of DPAs recently. By introducing techniques, such as, integrated compensating reactance [10], [11], post-matching structure [12]–[15], complex combining loads [16], [17], extended high efficiency operation modes [18]–[22] and reciprocal gate bias [23], the bandwidth of the DPA has been greatly extended. Although these techniques can improve the impedance matching condition of DPA, impedance mismatch at back-off region still exists due to limitations of their load modulation network (LMN) structures, which can decrease the efficiency performance and also affect the in-band consistency to some extent. It is therefore desirable to explore new LMN architectures to provide more precise impedance matching at power back-off within a wide frequency range while maintaining Doherty load modulation operation at the same time.

In this paper, a modified LMN architecture is proposed to provide close to ideal back-off impedance matching at OBO within a designed bandwidth for Doherty PAs. The analytical solution of the LMN parameters is given and the load modulation process of the DPA employing the proposed LMN is analyzed. A practical approximation method is also presented to simplify the design of the proposed LMN. It is illustrated that the proposed DPA can achieve very compact matching impedance at both OBO and saturation. A wideband DPA using commercial GaN devices with bandwidth of 2.8-3.55 GHz is designed and implemented based on the proposed LMN. For the fabricated DPA, the back-off efficiency of 55%-60% is achieved within 700 MHz bandwidth.

The remaining part of this paper is organized as follows, Section II demonstrates the operation principle of the proposed DPA using a modified LMN. Theoretical analysis of the proposed LMN and the related LMN parameters are given. Load modulation process of the DPA using the proposed LMN is also presented. Section III shows the detailed design procedure of realizing the proposed DPA with commercial GaN transistors on a 31 mil Rogers 5880 substrate. In Section IV, the measurement results and comparison with other state-of-art wideband DPAs are presented with a conclusion given in Section V.

This work was supported in part by the Science Foundation Ireland under Grant Numbers 13/RC/2077, 17/NSFC/4850 and 16/IA/4449. This research was also funded in part by funding from the European Union's Horizon 2020 Research and Innovation Program under the Marie Sklodowska-Curie grant agreement number 713567. (*Corresponding author: Jingzhou Pang*)

The authors are with the School of Electrical and Electronic Engineering, University College Dublin, Dublin 4, Ireland. (e-mail: meng.li@ucdconnect.ie; jingzhou.pang@ucd.ie; yue.li1@ucdconnect.ie; anding.zhu@ucd.ie)

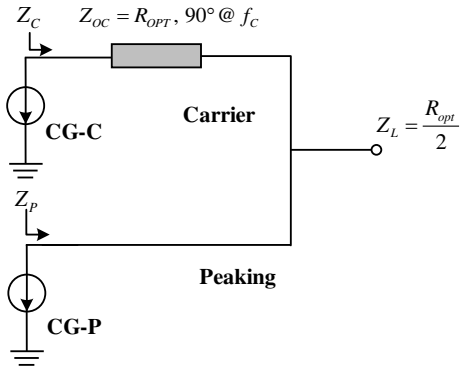

Fig. 1. The block diagram of the conventional DPA.

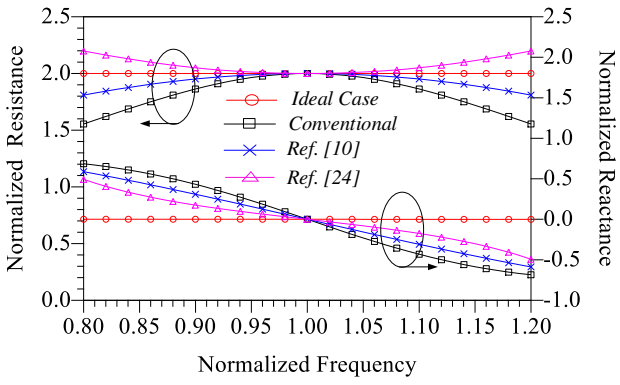

Fig. 2. The normalized resistance and reactance of Z_C in the ideal case, the conventional DPA, and the DPAs proposed in [10] and [24].

II. Theoretical Analysis of the Proposed DPA

The Doherty power amplifier is usually composed of a class-B biased carrier amplifier and a class-C biased peaking amplifier. The block diagram of the conventional DPA is shown in Fig. 1, in which the active devices are represented by using current generators (CGs) and Z_C and Z_P are the matching impedance of the carrier and peaking amplifiers. The load impedance Z_L is set to $R_{OPT}/2$, while R_{OPT} is the optimal impedance of the carrier and peaking devices. A quarter wavelength transmission line (TL) with the characteristic impedance of R_{OPT} is used as the impedance inverter to achieve load modulation. At high input power levels, both carrier and peaking amplifiers are active while the input power is low, only the carrier amplifier is active. The back-off efficiency is improved by using the quarter wavelength TL to provide impedance inversion during the active load modulation process. This solution is simple but the bandwidth of the conventional DPA is limited by the quarter wavelength TL due to its frequency dependent characteristics.

As mentioned earlier, it is very important to maintain high back-off efficiency for DPA. When considering the DPA operating in the linear region, the back-off efficiency can be simply calculated as,

$$\eta_{DE} = \frac{i_1^2 \cdot \text{real}(Z_{C,OBO})}{2 \cdot i_0 \cdot V_0} \tag{1}$$

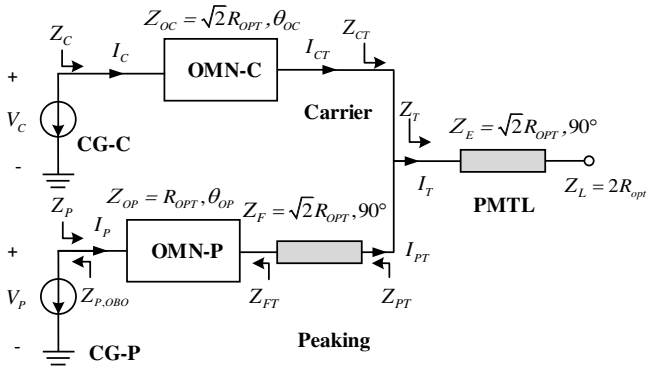

Fig. 3. Load modulation networks of the proposed DPA.

where $Z_{C,OBO}$ is the impedance of the carrier amplifier at back-off at the CG plane. i_0 and i_1 are the DC and fundamental current components which have the relationship of $i_1/i_0 = \pi/2$ for class-B mode power amplifiers. V_0 is the carrier DC supply voltage. From (1), we can see that the back-off efficiency of the DPA depends on the value of $Z_{C,OBO}$. For a wideband DPA, ideally, $Z_{C,OBO}$ should be kept at the same value, i.e.,

$$\begin{cases} \text{real}(Z_{C,OBO}) = 2R_{OPT} \\ \text{imag}(Z_{C,OBO}) = 0. \end{cases} \tag{2}$$

across a wide bandwidth, and thus a high back-off efficiency, e.g., 78.5%, can be achieved within the entire operation bandwidth. Due to the frequency dependent characteristics of the quarter wavelength TL, in the conventional DPA, this condition is difficult to satisfy because $Z_{C,OBO}$ changes when the operation frequency deviates from the center frequency, as shown in Fig. 2. In recent years, many works have been devoted to change the LMN structure to meet this condition, such as by employing impedance compensation technique [10] and introducing half wavelength off-set line in the peaking branch [24]. For comparison, the back-off impedance of the cases introduced in [10] and [24] are demonstrated. From Fig. 2, we can see that the impedance compensation techniques can improve the condition to some extent but the mismatch still exists when the operation frequency band becomes wider. This mismatch will decrease the efficiency performance and cause performance inconsistencies within the operation bandwidth.

A. Structure of the Proposed LMN

To satisfy the back-off impedance condition in (2), we propose a modified LMN with wideband feature as shown in Fig. 3. The proposed LMN consists of two wideband output matching networks (OMNs), an off-set line in the peaking branch and a post-matching transmission line (PMTL). In practical DPA design, the active transistor devices can not be simply treated as ideal current generators (CGs) since the parasitic and package parameters can not be ignored. These parameters must be considered as part of output matching network of the DPA. Therefore, two output matching networks, i.e., OMN-C and OMN-P, shown in Fig. 3, are employed

in the proposed LMN. In this configuration, OMN-C can be used as an equivalent TL impedance inverter with a specific phase characteristic while OMN-P provides the matching function for the peaking device. In the conventional DPA, The bandwidth is limited by the quarter wavelength TL impedance inverter due to its frequency dependent feature. It has been proven that, the bandwidth can be extended by introducing non-infinite peaking output impedance in DPA designs when the operation frequency deviates from the center [25]. In the proposed LMN, the non-infinite peaking output impedance can also be introduced by designing the phase of OMN-P. It should be noticed that, the phase shift of the entire peaking branch should be 180 degrees to ensure the infinite peaking output impedance at the centre frequency. To provide this phase shift, an off-set line is added in the peaking branch as shown in Fig. 3. Because the introduction of the above mentioned circuits changes the requirement for the combining load, a post-matching network should be added to maintain the Doherty operation. In the proposed LMN, the introduced PMTL provides this function. The two OMNs are assumed to be lossless two port networks and marched to Z_{OC} and Z_{OP} at each port in a desired frequency band. In this situation, Z_{OC} and Z_{OP} can be defined as the equivalent characteristic impedance of the carrier and peaking OMNs, OMN-C and OMN-P. The load of the proposed LMN Z_L is set to $2R_{OPT}$. To ensure the Doherty operation at the centre frequency, Z_{OC} and Z_{OP} are set to $\sqrt{2}R_{OPT}$ and R_{OPT}, respectively. Similarly, the characteristic impedance of the off-set line and PMTL are both set to $\sqrt{2}R_{OPT}$. The specific values of Z_{OC} and Z_{OP} are chosen to provide the minimum impedance ratio between the combining load and the CG planes at both back-off and saturation. Based on the above settings, the LMN parameters that need to be obtained in the proposed architecture are the phase of OMN-C, θ_{OC}, and the phase of OMN-P, θ_{OP}.

B. Analytical Solution of the proposed LMN Parameters

To obtain the analytic solution of the above mentioned LMN parameters by using condition (2), $Z_{C,OBO}$ should be expressed using the related LMN parameters. This expression can be obtained by using the characteristic of the two port network. For the two lossless OMNs shown in Fig. 3, the ABCD matrix can be described as,

$$\begin{bmatrix} A & B \\ C & D \end{bmatrix} = \begin{bmatrix} \cos\theta & jZ_0\sin\theta \\ j\dfrac{\sin\theta}{Z_0} & \cos\theta \end{bmatrix} \tag{3}$$

where Z_0 and θ are the equivalent characteristic impedance and phase of the OMNs, respectively. In addition, the matching impedance at the CG plane of these OMNs Z_{CG} can be expressed as,

$$Z_{CG} = \frac{Z_{OMN}A + B}{Z_{OMN}C + D} \tag{4}$$

where Z_{OMN} is the impedance at the other port of the OMN.

From (3) and (4), the carrier matching impedance Z_C can be derived as,

$$Z_C = Z_{OC}\frac{Z_{CT} + jZ_{OC}\tan\theta_{OC}}{Z_{OC} + jZ_{CT}\tan\theta_{OC}} \tag{5}$$

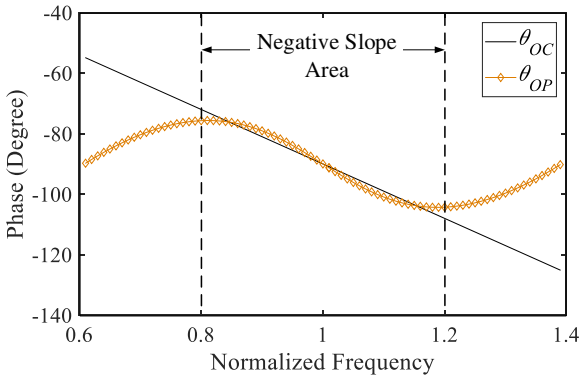

Fig. 4. θ_{OC} and θ_{OP} versus normalized frequency from 0.6 to 1.4.

where Z_{CT} is the carrier impedance at the combining point, and can be calculated as follows at OBO,

$$Z_{CT,OBO} = Z_T // Z_{PT,OBO}. \tag{6}$$

Based on the characteristics of quarter wavelength TLs, Z_T and $Z_{PT,OBO}$ can be derived as follows,

$$Z_T = Z_E\frac{Z_L + jZ_E\tan(\frac{\pi}{2}f)}{Z_E + jZ_L\tan(\frac{\pi}{2}f)} \tag{7}$$

$$Z_{PT,OBO} = Z_F\frac{Z_{FT,OBO} + jZ_F tan(\frac{\pi}{2}f)}{Z_F + jZ_{FT,OBO}tan(\frac{\pi}{2}f)}. \tag{8}$$

At OBO, since the peaking PA is turned off, the output impedance at the peaking CG plane thus is,

$$Z_{P,OBO} = \infty. \tag{9}$$

From (9) and (4), $Z_{FT,OBO}$ can be calculated as follows,

$$Z_{FT,OBO} = Z_{OP}\frac{1}{j\tan\theta_{OP}}. \tag{10}$$

Therefore, from the above equations, $Z_{C,OBO}$ can be expressed as,

$$Z_{C,OBO} = \sqrt{2}R_{OPT}\frac{\gamma + j\tan\theta_{OC}}{1 + j\gamma\tan\theta_{OC}} \tag{11}$$

where γ and δ are defined as,

$$\begin{cases} \gamma = \dfrac{-\delta\tan(\frac{\pi}{2}f) + j\sqrt{2}\delta}{\sqrt{2} - \sqrt{2}\delta\tan(\frac{\pi}{2}f) + j\tan(\frac{\pi}{2}f) + j\delta} \\ \delta = \dfrac{\sqrt{2}\tan\theta_{OP}\tan(\frac{\pi}{2}f) - 1}{\tan(\frac{\pi}{2}f) + \sqrt{2}\tan\theta_{OP}}. \end{cases} \tag{12}$$

In the expression of $Z_{C,OBO}$, only θ_{OC} and θ_{OP} are unknown. By using the impedance condition in (2), θ_{OC} and θ_{OP} can be solved as follows,

$$\begin{cases} \theta_{OC} = \dfrac{\pi}{2}f \\ \theta_{OP} = \arctan(\dfrac{\tan^3(\frac{\pi}{2}f) + 4\cdot\tan(\frac{\pi}{2}f)}{2\sqrt{2} - \sqrt{2}\cdot\tan^2(\frac{\pi}{2}f)}) \end{cases} \tag{13}$$

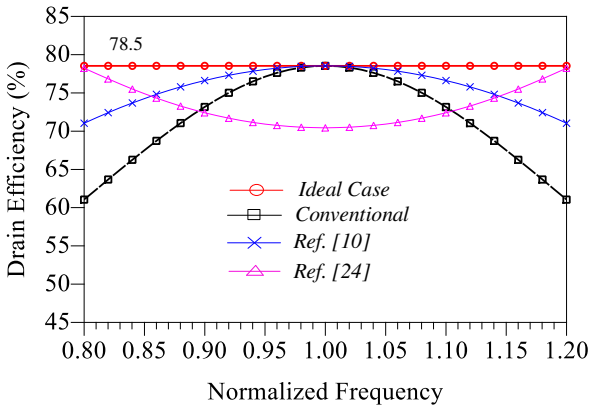

Fig. 5. Back-off drain efficiency of the proposed DPA and conventional DPAs with respect to normalized frequency.

In this expression, the center frequency is defined as the frequency when θ_{OC} equals to $-\pi/2$. When f is normalized to the center frequency, the value of θ_{OC} and θ_{OP} versus frequency can be depicted as shown in Fig. 4. From Fig. 4 we can see, that θ_{OC} is linear with frequency and θ_{OP} is nonlinear. For θ_{OP}, the phase increases first and then decreases and then arises again, when the normalized frequency changes from 0.6 to 1.4. It means that we have to find a matching network to achieve a phase slope which changes from positive to negative. It is difficult to achieve this phase relationship in actual circuits. In this work, the negative slope frequency range is chosen for the proposed LMN design. This frequency range can be simply calculated by solving the following equation,

$$\frac{\mathrm{d}\theta_{OP}(f)}{\mathrm{d}f} = 0 \tag{14}$$

From (14), the normalized frequency range with the negative phase slope is from 0.8 to 1.2. Within this frequency range, θ_{OC} changes from $-72°$ to $-108°$, while θ_{OP} changes from $-75.7°$ to $-104.3°$. Once the phase characteristics of θ_{OC} and θ_{OP} are achieved, the ideal back-off impedance shown in Fig. 2 can be obtained. As mentioned early, when this condition is satisfied, the efficiency of the proposed DPA within the designed bandwidth will keep constant to the ideal case as shown in Fig. 5. The drain efficiency of the conventional DPA and the DPAs introduced in [10] and [24] at OBO are also given in Fig. 5 as comparison. It can bee seen that the proposed DPA shows the best efficiency performance theoretically.

C. Load Modulation Process Analysis of Proposed DPA

The above analysis gives the analytical solution of the proposed LMN based on the back-off impedance condition (2). It should be noticed that this condition only guarantees the performance at OBO. Therefore, to ensure the Doherty operation, the entire load modulation process when the peaking amplifier turns on should be discussed. For the proper load modulation process, due to the increased current ratio of peaking and carrier, Z_C will decrease from $2R_{OPT}$ to R_{OPT} while Z_P will decrease from infinity to R_{OPT}. For the symmetric DPA, the peaking PA turns on when the carrier PA generates half of its maximum power. Thus, mathematically, the relationship between normalized carrier and peaking current (I_C and I_P) in the proposed DPA can be defined as follows,

$$I_P = \begin{cases} 0, & 0 \le |I_C| \le 0.5 \\ 2I_C \cdot e^{j\frac{\pi}{2}f} - 1, & 0.5 \le |I_C| \le 1 \end{cases} \tag{15}$$

where $I_P/I_C = (|I_P|/|I_C|) \cdot e^{j\frac{\pi}{2}f}$, $e^{j\frac{\pi}{2}f}$ is the phase difference between the carrier and peaking currents which can be provided by a quarter wavelength TL added in front of the carrier input matching network (IMN). Let's assume $|I_P|/|I_C| = \alpha$ and we can see that α will change from 0 to 1 through the load modulation process. With the change of the current ratio, the matching impedance of peaking and carrier will also change. To obtain the carrier and peaking matching impedance during the load modulation process, the voltage and current relationship at the CG plane and the combining node should be discussed.

In terms of the ABCD parameter of OMN-C, the following relationship between V_C and I_C can be obtained as,

$$\begin{bmatrix} V_C \\ I_C \end{bmatrix} = \begin{bmatrix} A_C & B_C \\ C_C & D_C \end{bmatrix} \begin{bmatrix} V_{CT} \\ I_{CT} \end{bmatrix} \tag{16}$$

where the matrix $ABCD_C$ can be expressed as,

$$\begin{bmatrix} A_C & B_C \\ C_C & D_C \end{bmatrix} = \begin{bmatrix} \cos\theta_{OC} & j\sqrt{2}R_{OPT}\sin\theta_{OC} \\ j\dfrac{\sin\theta_{OC}}{\sqrt{2}R_{OPT}} & \cos\theta_{OC} \end{bmatrix}. \tag{17}$$

Moreover, according to the current and voltage relationship at the combining point, V_{CT} can be expressed by I_{CT} and I_{PT},

$$V_T = V_{CT} = V_{PT} = (I_{CT} + I_{PT})Z_T. \tag{18}$$

Thus, from (16) and (18), V_C and I_C can be calculated as,

$$\begin{cases} V_C = A_C Z_T(I_{CT} + I_{PT}) + B_C I_{CT} \\ I_C = C_C Z_T(I_{CT} + I_{PT}) + D_C I_{CT}. \end{cases} \tag{19}$$

For the peaking branch, we can similarly obtain the relationship between the voltage and current as,

$$\begin{bmatrix} V_P \\ I_P \end{bmatrix} = \begin{bmatrix} A_P & B_P \\ C_P & D_P \end{bmatrix} \begin{bmatrix} V_{PT} \\ I_{PT} \end{bmatrix}. \tag{20}$$

Because the modified peaking output branch is made up of OMN-P and an off-set line, the ABCD matrix of the peaking output network is the multiplication of the ABCD matrices of the two networks and can be expressed as,

$$\begin{cases} A_P = \cos\theta_{OP}\cos(\frac{\pi}{2}f) - \frac{1}{\sqrt{2}}\sin\theta_{OP}\sin(\frac{\pi}{2}f) \\ B_P = jR_{OPT}(\sqrt{2}\cos\theta_{OP}\sin(\frac{\pi}{2}f) + \sin\theta_{OP}\cos(\frac{\pi}{2}f)) \\ C_P = j\frac{1}{R_{OPT}}(\sin\theta_{OP}\cos(\frac{\pi}{2}f) + \frac{1}{\sqrt{2}}\cos\theta_{OP}\sin(\frac{\pi}{2}f)) \\ D_P = \cos\theta_{OP}\cos(\frac{\pi}{2}f) - \frac{1}{\sqrt{2}}\sin\theta_{OP}\sin(\frac{\pi}{2}f) \end{cases} \tag{21}$$

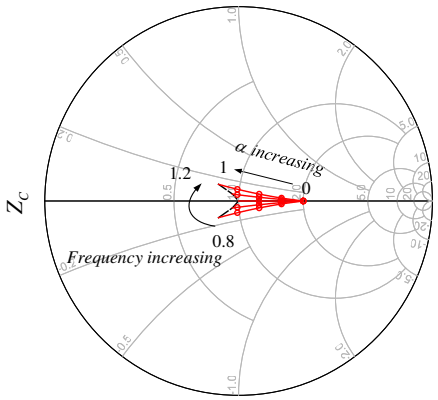

Fig. 6. Z_C modulation trajectories on the Smith chart within normalized frequency from 0.8 to 1.2.

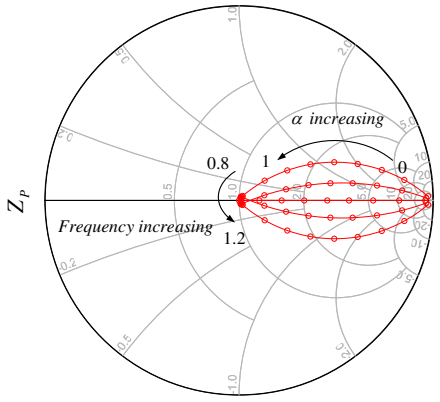

Fig. 7. Z_P modulation trajectories on the Smith chart within normalized frequency from 0.8 to 1.2.

From (20) and (18), V_P and I_P can be expressed as,

$$\begin{cases} V_P = A_P Z_T (I_{PT} + I_{CT}) + B_P I_{PT} \\ I_P = C_P Z_T (I_{PT} + I_{CT}) + D_P I_{PT} \end{cases} . \quad (22)$$

From above analysis, we hope V_C and V_P could be expressed by I_C and I_P so we can give the expression of Z_C and Z_P. However, from the expressions of V_C and V_P in (19) and (22) we can see, I_{CT} and I_{PT} are also in the expressions. To eliminate I_{CT} and I_{PT} in the voltages expressions, we can combine the expressions of I_C in (19) and I_P in (22). I_{CT} and I_{PT} can be solved as follows,

$$\begin{cases} I_{CT} = \dfrac{(C_P Z_T + D_P) I_C - C_C Z_T I_P}{C_C Z_T D_P + D_C D_P + D_C C_P Z_T} \\ I_{PT} = \dfrac{(C_C Z_T + D_C) I_P - C_P Z_T I_C}{C_C Z_T D_P + D_C D_P + D_C C_P Z_T} \end{cases} . \quad (23)$$

Now, we can replace I_{CT} and I_{PT} in the expressions of V_C and V_P by substituting (23) into (19) and (22). Z_C and Z_P are derived by V_C/I_C and V_P/I_P as,

$$\begin{cases} Z_C = (A_C Z_T (D_P + D_C \dfrac{I_P}{I_C}) + B_C (C_P Z_T + D_P) \\ -B_C C_C Z_T \dfrac{I_P}{I_C}) / (C_C Z_T D_P + D_C D_P + D_C C_P Z_T) \\ Z_P = (A_P Z_T (D_P \dfrac{I_C}{I_P} + D_C) + B_P (C_C Z_T + D_C) \\ -B_P C_P Z_T \dfrac{I_C}{I_P}) / (C_C Z_T D_P + D_C D_P + D_C C_P Z_T) \end{cases} \quad (24)$$

where $I_P/I_C = \alpha \cdot e^{\frac{\pi}{2} f}$. Once the expression of Z_C and Z_P are obtained, we only need to sweep the value of α in (24) from 0 to 1, then the matching impedance in the load modulation process of proposed DPA can be presented. In addition, we can also obtain the load modulation characteristic at different operation frequencies.

When the frequency deviates from the center frequency, the load modulation process of Z_C with α varying from 0 to 1 can be demonstrated as shown in Fig. 6. From the results we can see, that the carrier matching impedance maintains

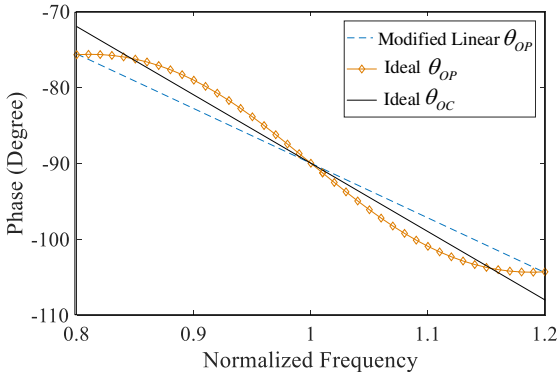

Fig. 8. The modified linear θ_{OP} versus normalized frequency from 0.8 to 1.2.

concentrated within the normalized frequency from 0.8 to 1.2 in the whole load modulation process. When α is changed from 0 to 1, Z_C is changed from $2R_{OPT}$ to a series of values very close to R_{OPT}. It means that the voltage saturation can be kept and the highest efficiency can be maintained. It should be noticed that the carrier matching impedance at saturation is not as compact as that at OBO. This degree of divergence can lead to some power loss, but the loss is small and thus is usually acceptable. Similarly, the load modulation of Z_P is depicted in Fig. 7. It can be seen that the peaking matching impedance at OBO and saturation is very compact within the desired bandwidth. When α is changed from 0 to 1, Z_P is changed from infinity to a series of values those also are very close to R_{OPT}. It means that, at saturation, the peaking PA can provide equal power as the carrier one and make the DPA maintain high efficiency performance in the desired bandwidth.

D. Practical Design Consideration

From the above analysis we can see, the required θ_{OP} decreases from $-75.7°$ to $-104.3°$ when the normalized frequency changes from 0.8 to 1.2, but not linear with the frequency in this frequency range. It should be noticed that, this specific phase characteristic is difficult to realize. In [23], [26], OMNs with approximate linear phase characteristic are

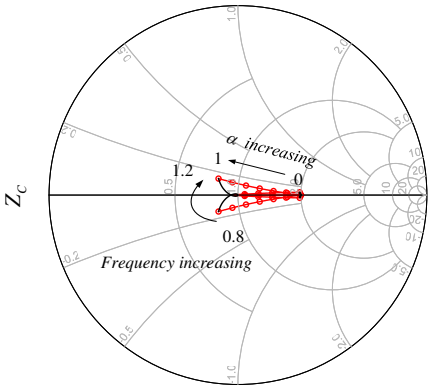

Fig. 9. Z_C modulation trajectories on the Smith chart with the modified linear θ_{OP}.

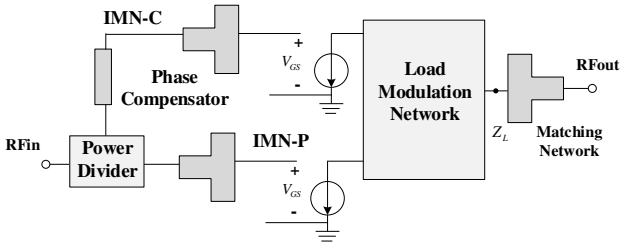

Fig. 10. Block diagram of the proposed DPA.

proven to be effective for designing wideband DPAs. Therefore, it is attractive to discuss if we can simplify θ_{OP} using a linear function while maintain similar Doherty operation for the proposed DPA. According to the range of the ideal θ_{OP} that we solved in (13), θ_{OP} can be modified to a linear function as,

$$\theta_{OP} = \frac{0.8\pi}{2} f + \frac{0.2\pi}{2}. \tag{25}$$

The modified linear θ_{OP} is shown in Fig. 8. In this linear function, we keep the minimum and maximum of the ideal θ_{OP} unchanged. Using the same method described in the previous subsection, the modulation process of Z_C with the modified θ_{OP} can be demonstrated in Fig. 9. The matching impedance of the carrier at OBO is no longer concentrated on one point but still very close to $2R_{OPT}$. In terms of Z_C at saturation, the same as that shown in Fig. 6, the carrier resistance is smaller than the ideal value while the reactance exists at the same time. This imperfect impedance will decrease the saturated efficiency and output power to some extent [25]. Nevertheless, because the carrier impedance just has a small deviation from the ideal value, the performance degradation caused by it will be acceptable.

From the above analysis we can see, that the proposed DPA not only has a wideband feature at OBO, but also maintains this feature at saturation. Moreover, from (23), the defined phase difference between the carrier and peaking PAs is $-\pi/2$ at the center operation frequency, which can be realized by introducing a 50 Ω quarter wavelength TL in front of the input matching network (IMN) of the carrier amplifier. Besides, a post matching network is required to achieve $2R_{OPT}$ to 50 Ω matching after the PMTL. Because there is no load modulation process in the post-matching network, it is easy to design this network within the desired bandwidth. The block diagram of the proposed DPA can be built as shown in Fig. 10.

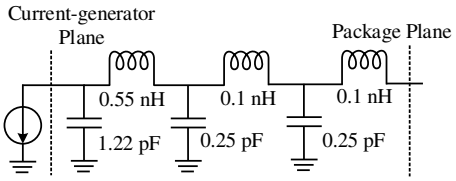

Fig. 11. Equivalent parasitic model of package of CGH40010F.

III. Design of the Proposed DPA

To demonstrate the proposed design, commercial GaN HEMTs CGH40010F transistors from Wolfspeed were used. The DPA was fabricated on 31 mil Rogers 5880 substrates with dielectric constant of 2.2. The drain supply voltage V_{DS} was set to 28 V. The maximum current of the device was 1.5 A. Thus, R_{OPT} of the used device was estimated to 32 Ω considering the knee voltage was about 4 V [14]. The designed band of the proposed DPA was from 2.95 GHz to 3.65 GHz. To design the LMN for the proposed DPA, the transistor model should be de-embeded first because the discussion in Section II is based on the calculation at the current generator plane. The circuit introduced in [27] was used to model the parasitic and package as shown in Fig. 11. According to the block diagram shown in Fig. 10, the circuits details of the proposed DPA could be realized as shown in Fig. 12. The design details are given as follows.

Firstly, based on the analysis in Section II, the OMN-C and OMN-P were realized with the consideration of absorbing the parasitic parameters of transistors. The target value of Z_{OC} and Z_{OP} was equal to $\sqrt{2}R_{OPT}$ and R_{OPT}, which was 45 Ω and 32 Ω, respectively. The target θ_{OC} and θ_{OP} were $-90°$ at 3.3 GHz. Considering including the drain bias lines for carrier and peaking PAs in both OMN-C and OMN-P, the T-shape TL structures were employed as shown in Fig. 12. As the target was simple, the specific parameters of the TLs were directly optimized to achieve the required matching impedance and phase relationship with the load value of $\sqrt{2}R_{OPT}$ and R_{OPT}. The designed phases and impedance trajectories of OMN-C and OMN-P are shown in Fig. 13. From Fig. 13 (a), the phase of OMN-C is changed from $-74°$ to $-105°$, while the phase of OMN-P is changed from $-77°$ to $-102°$. This is very consistent with what we solved in Section II. In addition, the designed Z_{OC} and Z_{OP} are shown in Fig. 13(b) on Smith Chart with the reference impedance of 45 Ω and 32 Ω. It can be seen that the trajectories of Z_{OC} and Z_{OP} are concentrated to the center of the Smith Chart with the frequency range from 2.95 GHz to 3.65 GHz. These results show the designed OMNs satisfy the requirement of the proposed OMNs.

Secondly, the PMTL and peaking off-set line with impedance of Z_F were designed. PMTL was realized by using

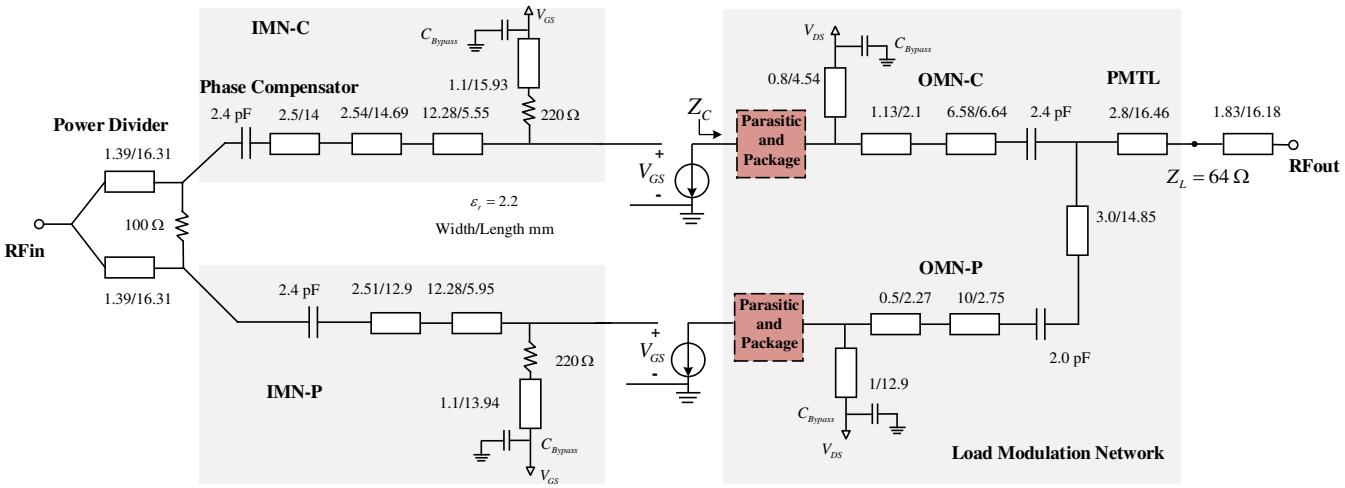

Fig. 12. Circuits details of the proposed DPA.

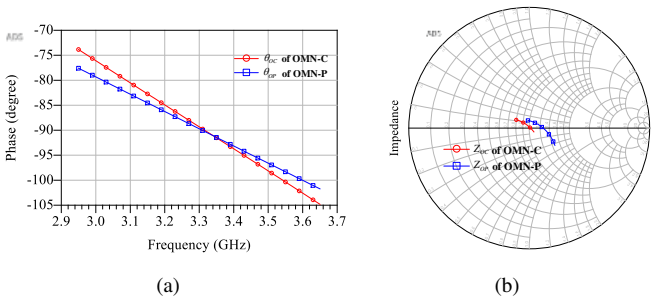

Fig. 13. Designed phases and characteristic impedance for the OMN-C,P from 2.95 GHz to 3.65 GHz (a) θ_{OC} and θ_{OP} (b) Z_{OC} and Z_{OP} trajectories on the Smith chart.

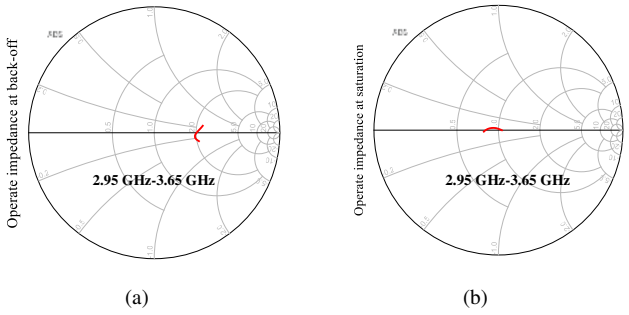

Fig. 14. Designed Z_C from 2.95 GHz to 3.65 GHz (a) at OBO and (b) at saturation.

a 90° TL with characteristic impedance of 64 Ω as shown in Fig. 12. Z_F was realized by using a 90° TL with characteristic impedance of 64 Ω after OMN-P. In practice, due to the non-ideal DC blocking capacitors and the difference between the actual circuits and theoretical assumptions, PMTL and off-set line should be slightly adjusted. After the output network of the proposed DPA had been designed, the designed Z_C at OBO and saturation can be obtained as shown in Fig. 14 on the Smith Chart with the reference impedance of 32 Ω. From

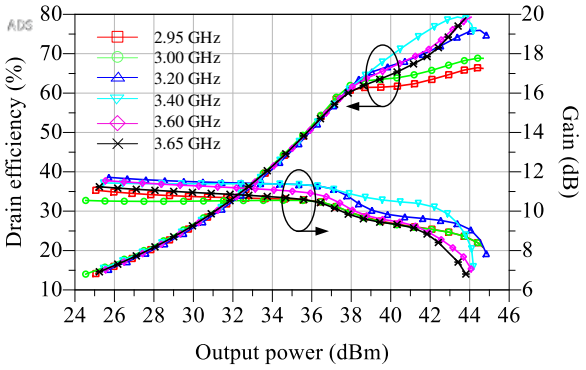

Fig. 15. Simulated drain efficiencies and gains of the fabricated DPA versus output power at different frequencies.

Fig. 14 we can see, that Z_C is close to $2R_{OPT}$ at OBO and R_{OPT} at saturation. The result is in a good agreement with that derived from the theory.

Thirdly, because the different modes are utilized for carrier and peaking amplifier, the different input matching networks (IMNs) should be designed for them. Stepped TL structure were employed to realized IMNs. A 50 Ω TL was then applied in front of the IMN-C to compensate the phase difference between the two amplifiers. Besides, a 3 dB Wilkinson divider was employed at input to split the input signal.

The EM simulation of the entire DPA was run in ADS Momentum from Keysight. The V_{GS} of carrier was set to -2.95 V with the quiescent current 70 mA, while the V_{GS} of peaking was set to -6.2 V. The simulated drain efficiency and gain of the proposed DPA versus the output power are presented in Fig. 15. From Fig. 15 we can see, that higher than 60.0% drain efficiency (DE) can be achieved at 6 dB back-off across the designed band. Besides, 66.0% to 79.0% DE can be achieved at saturation with the output power from 44 dBm to 45.0 dBm. In addition, the DPA achieves gain compression of 2.3 dB to 4.0 dB at saturation. To better illustrate the simulated

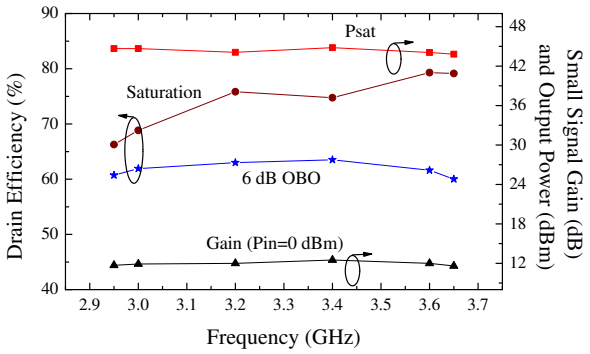

Fig. 16. Simulated drain efficiency, output power and gain versus frequency at 2.95-3.65 GHz.

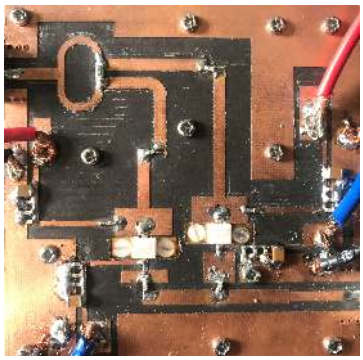

Fig. 17. Fabricated PCB circuit of the designed DPA.

performance of the DPA cross a wide bandwidth, the simulated results versus frequency from 2.95-3.65 GHz are shown in Fig. 16.

From the above simulation results we can see that the Doherty operation can be obviously achieved by the proposed DPA. It should be noticed that, the efficiency and gain curves are almost flat across a wide bandwidth, especially at OBO region. This means the designed DPA presents consistent performance within the designed band, which greatly benefits the linearity of the DPA when driven by wideband modulated signals.

IV. Measurement Results

The photo of the fabricated circuits of the proposed DPA is shown in Fig. 17. The DPA was measured using both continuous-wave (CW) and wideband modulated signals. The tested frequency band was from 2.80 GHz to 3.55 GHz. The fabricated DPA has a frequency shift of 100 MHz compared with the simulation, which might be caused by the model and fabrication inaccuracies. In the measurements, the CW and modulated signals were both generated by a vector signal generator, and the output power was tested by a spectrum analyzer. A broadband linear driver was used to amplify the input signal to the required power level. During all the measurements, the proposed DPA was biased with carrier quiescent current of 70 mA and peaking gate DC voltage of -6.6 V. The drain supply voltages of the carrier and peaking PAs were both set to 28 V.

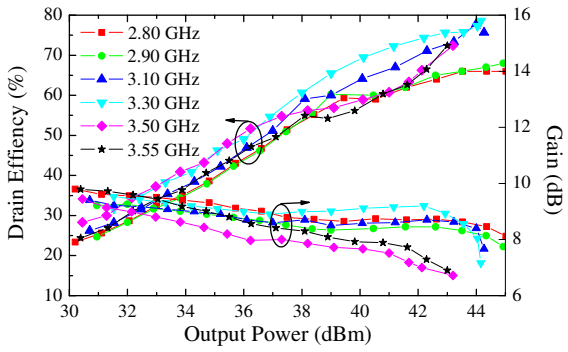

Fig. 18. Measured drain efficiency and gain versus the output power at 2.80-3.55 GHz.

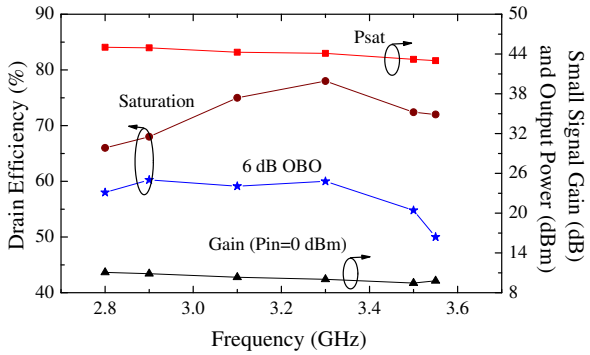

Fig. 19. Measured drain efficiency, output power and gain versus frequency at 2.80-3.55 GHz.

A. Measurement Results with CW Signals

The fabricated DPA was firstly measured using CW signals. Fig. 18 shows the measured drain efficiency and gain versus the output power at different operation frequencies. It can be seen that Doherty operation was achieved in the measured band. The proposed DPA achieves drain efficiency from 50.0% to 60.6% at 6 dB OBO region from 2.80 GHz to 3.55 GHz. To better present the wideband performance of the proposed DPA, the measured drain efficiency, maximum output power and gain versus operation frequency are presented in Fig. 19. From the results, we can see that the DE curve at 6 dB OBO is fairly flat from 2.80 GHz to 3.5 GHz. It is worth noticing that within 700 MHz bandwidth, the back-off drain efficiency of the fabricated DPA is higher than 55%. It is consistent with our theory analyzed in Section II. For the saturation, the DE of 66.0% to 78.0% is achieved. Moreover, maximum output power of 43.2 dBm to 45.0 dBm is achieved with small signal gain from 9.3 dB to 11.1 dB. From the results, we can see that the measured efficiency and output power are slightly lower than that in simulation and the operation frequency of the fabricated DPA also slightly deviates from that in simulation. This might be caused by the inaccuracy of the transistor model especially that in class-C operation [12]. The fabrication accuracy also affects the measured results to a certain extent. Nevertheless, the measurement results matched with that in simulation reasonably well within the desired frequency band.

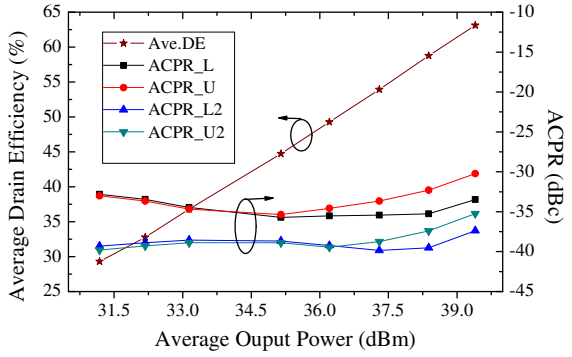

Fig. 20. Measured average efficiency and ACPR versus output power under 40 MHz 6.5 dB PAPR OFDM signal stimulation at 3.20 GHz.

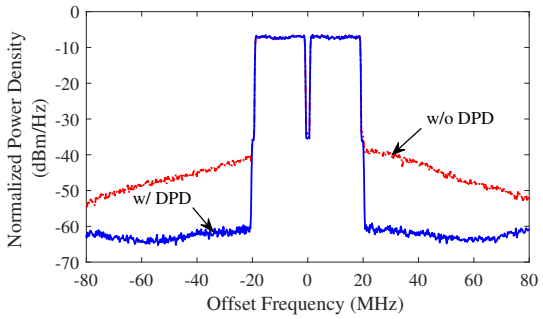

Fig. 21. Output Spectrum under 40 MHz 6.5 dB PAPR OFDM signal stimulation at 3.20 GHz.

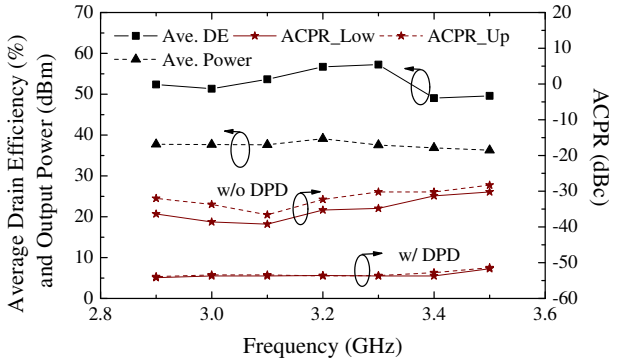

Fig. 22. Measured average DE and ACPR at 2.9-3.5 GHz using the 2-Carrier 40 MHz OFDM Signal.

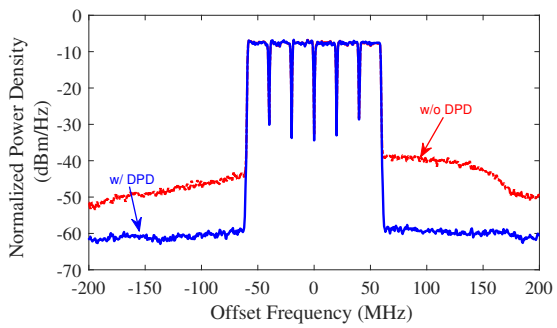

Fig. 23. Output Spectrum under 120 MHz 7.0 dB PAPR OFDM signal stimulation with 37.3 dBm at 3.20 GHz.

B. Measurement Results with Modulated Signals

To evaluate the capability of the proposed DPA under modulated signal stimulation, two OFDM signals with different signal bandwidth were employed for the measurement. Firstly, the fabricated DPA was measured using a 40 MHz signal with 6.5 dB PAPR at different output power levels and operation frequencies. Fig. 20 shows the measured average drain efficiency and adjacent channel power ratio (ACPR) versus the average output power at 3.20 GHz. It can be seen that the proposed DPA presents excellent average drain efficiency performance and also good linearity. The measured average output power changes from 31.2 dBm to 39.4 dBm while the ACPR maintains better than -30.3 dBc. At 39.4 dBm, the average efficiency achieves 63.1%.

Digital pre-distortion (DPD) was then applied to correct the non-linearity of the proposed DPA at the same frequency. The linearity performance was measured using the Magnitude-Selective Affine (MSA) function model [28] and the proposed DPA was linearized with a closed-loop estimator. With DPD, the ACPR was improved from -35.3/-32.3 dBc to -53.6/-53.7 dBc at 3.2 GHz as shown in Fig. 20. The related average output power was 38.4 dBm and the average drain efficiency was 56.7%. More measured results under the 40 MHz OFDM signal with 6.5 dB PAPR are given in Fig. 22. After DPD, the fabricated DPA had average drain efficiency of 49.1%-57.2% and ACPR better than -51.4 dBc from 2.9 GHz to 3.5 GHz.

To further demonstrate the performance of the proposed DPA under wideband signal stimulation, another measurement under a 6-carrier 120 MHz OFDM signal with 7.0 dB PAPR was performed at 3.20 GHz. Fig. 23 shows the output spectrum with and without DPD at 3.20 GHz. The average drain efficiency of 53.3% was achieved with 37.3 dBm average output power. The ACPR was improved from - 36.1/-30.1 dBc to -50.7/-50.4 dBc. The AM/AM and AM/PM under 120 MHz OFDM signal stimulation are shown in Fig. 24, where we can see that the non-linearity can be effectively corrected after DPD is performed.

C. Performance Comparison

Table I summarizes the performance comparison of some recently reported wideband PAs with high back-off efficiency performance. η_{sat} and η_{bo} represent the drain efficiency at saturation and 6 dB OBO. It can be seen that, compared with the other published PAs, the proposed DPA demonstrates excellent efficiency performance at both the OBO region and saturation while attains comparable bandwidth performance.

V. Conclusion

A new DPA architecture with extended bandwidth and back-off efficiency by using a modified LMN has been proposed in this paper. Compact back-off impedance can be achieved by employing the proposed LMN. The analytical solution of the LMN parameters and the load modulation process of the proposed DPA were presented. The proposed DPA was designed by using commercial GaN transistor within 2.80 GHz

TABLE I
PERFORMANCE COMPARISON

Ref	Freq (GHz)	Pout (dBm)	Gain (dB)	η_{sat} (%)	η_{bo} (%)	B.W. (%)	Technology	Architecture
[5]	1.8-2.7	40.5-41.4	8.9-13.0	54-73	47.5-54.0	20	GaN	Doherty
[10]	1.7-2.8	44-44.5	13.2-15.7	57-71	50-55	48	GaN	Doherty
[12]	1.7-2.6	44.6-46.3	10.2-11.6	57-66	47-57	41.8	GaN	Doherty
[20]	1.65-2.75	44.5-46.3	9.3-11.7	60-77	52-66	50	GaN	Doherty
[29]	3.0-3.6	43-44	8-11	55-66	38-56	18.2	GaN	Doherty
[30]	4.7-5.3	39.0-39.5	7-7.5	52-67	29.7-33.1	12	GaN	Doherty
[31]	1.8-3.8	42-44	7.5-11	37-59*	29-45*	71.4	GaN	LMBA
[32]	1.5-3.8	42.3-43.4	8-11	42-63	33-55	87	GaN	Doherty
This Work	**2.80-3.55**	**43.0-45.0**	**8.3-9.1**	**66-78/ 55.8-63.5***	**50.0-60.6/ 42.8-53.0***	**23.62**	**GaN**	**Doherty**

* Power added efficiency

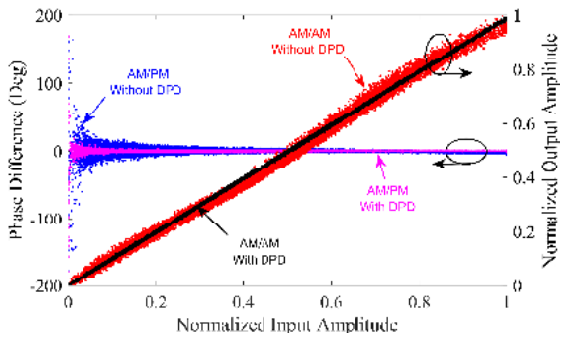

Fig. 24. AM/AM and AM/PM under 120 MHz 7.0 dB PAPR OFDM signal stimulation at 3.20 GHz.

to 3.55 GHz band. Measured drain efficiencies of 55%-60% were achieved at 6 dB back-off within 700 MHz bandwidth. From the simulation and measurements results, we can see that, the proposed DPA can achieve high efficiency at back-off region with wideband performance. The proposed architecture provides a promising solution for high efficiency PAs for wideband applications.

REFERENCES

[1] P. Chen and S. He, "Investigation of inverse class-E power amplifier at sub-nominal condition for any duty ratio," *IEEE Trans. Circuits Syst. I Reg. Papers*, vol. 62, no. 4, pp. 1015–1024, Apr. 2015.

[2] J. Pang, S. He, C. Huang, Z. Dai, C. Li, and J. Peng, "A novel design of concurrent dual-band high efficiency power amplifiers with harmonic control circuits," *IEEE Microw. Wirel. Compon. Lett.*, vol. 26, no. 2, pp. 137–139, Feb. 2016.

[3] C. Li, F. You, S. He, X. Tang, W. Shi, and J. Wang, "High-efficiency power amplifier employing minimum-power harmonic active load modulator," *IEEE Trans. Circuits Syst. II Express Briefs*, vol. 66, no. 8, pp. 1371–1375, Aug. 2019.

[4] Z. Dai, S. He, J. Peng, C. Huang, W. Shi, and J. Pang, "A semianalytical matching approach for power amplifier with extended chebyshev function and real frequency technique," *IEEE Trans. Microw. Theory Techn.*, vol. 65, no. 10, pp. 3892–3902, Oct. 2017.

[5] X. Y. Zhou, S. Y. Zheng, W. S. Chan, S. Chen, and D. Ho, "Broadband efficiency-enhanced mutually coupled harmonic postmatching Doherty power amplifier," *IEEE Trans. Circuits Syst. I Reg. Papers*, vol. 64, no. 7, pp. 1758–1771, Jul. 2017.

[6] W. Chen, S. Zhang, Y. Liu, Y. Liu, and F. M. Ghannouchi, "A concurrent dual-band uneven Doherty power amplifier with frequency-dependent input power division," *IEEE Trans. Circuits Syst. I Reg. Papers*, vol. 61, no. 2, pp. 552–561, Feb. 2014.

[7] X. A. Nghiem, J. Guan, T. Hone, and R. Negra, "Design of concurrent multiband Doherty power amplifiers for wireless applications," *IEEE Trans. Microw. Theory Techn.*, vol. 61, no. 12, pp. 4559–4568, Dec. 2013.

[8] S. Y. Zheng, Z. W. Liu, Y. M. Pan, Y. Wu, W. S. Chan, and Y. Liu, "Bandpass filtering doherty power amplifier with enhanced efficiency and wideband harmonic suppression," *IEEE Trans. Circuits Syst. I Reg. Papers*, vol. 63, no. 3, pp. 337–346, Mar. 2016.

[9] Qualcomm Technologies, "Spectrum for 4G and 5G," 2017. [Online]. Available: https://www.qualcomm.com/media/documents/files/spectrum-for-4g-and-5g.pdf

[10] J. Xia, M. Yang, Y. Guo, and A. Zhu, "A broadband high-efficiency Doherty power amplifier with integrated compensating reactance," *IEEE Trans. Microw. Theory Techn.*, vol. 64, no. 7, pp. 2014–2024, Jul. 2016.

[11] J. Xia, W. Chen, F. Meng, C. Yu, and X. Zhu, "Improved three-stage Doherty amplifier design with impedance compensation in load combiner for broadband applications," *IEEE Trans. Microw. Theory Tech.*, vol. 67, no. 2, pp. 778–786, Feb. 2019.

[12] J. Pang, S. He, C. Huang, Z. Dai, J. Peng, and F. You, "A post-matching Doherty power amplifier employing low-order impedance inverters for Broadband Applications," *IEEE Trans. Microw. Theory Techn.*, vol. 63, no. 12, pp. 4061–4071, Dec. 2015.

[13] X. Y. Zhou, S. Y. Zheng, W. S. Chan, X. Fang, and D. Ho, "Postmatching Doherty power amplifier with extended back-off range based on self-generated harmonic injection," *IEEE Trans. Microw. Theory Techn.*, vol. 66, no. 4, pp. 1951–1963, Apr. 2018.

[14] J. Pang, S. He, Z. Dai, C. Huang, J. Peng, and F. You, "Design of a post-matching asymmetric Doherty power amplifier for broadband applications," *IEEE Microw. Wirel. Compon. Lett.*, vol. 26, no. 1, pp. 52–54, Jan. 2016.

[15] H. Kang, H. Lee, W. Lee, H. Oh, W. Lim, H. Koo, C. Park, K. C. Hwang, K. Lee, and Y. Yang, "Octave bandwidth Doherty power amplifier using multiple resonance circuit for the peaking amplifier," *IEEE Trans. Circuits Syst. I Reg. Papers*, vol. 66, no. 2, pp. 583–593, Feb. 2019.

[16] X. Fang, H. Liu, K. M. Cheng, and S. Boumaiza, "Modified Doherty amplifier with extended bandwidth and back-off power range using optimized peak combining current ratio," *IEEE Trans. Microw. Theory Techn.*, vol. 66, no. 12, pp. 5347–5357, Dec. 2018.

[17] Z. Yang, Y. Yao, M. Li, Y. Jin, T. Li, Z. Dai, F. Tang, and Z. Li, "Bandwidth extension of Doherty power amplifier using complex combining

load with noninfinity peaking impedance," *IEEE Trans. Microw. Theory Tech.*, vol. 67, no. 2, pp. 765–777, Feb. 2019.
[18] J. Kim, J. Moon, Y. Y. Woo, S. Hong, I. Kim, J. Kim, and B. Kim, "Analysis of a fully matched saturated Doherty amplifier with excellent efficiency," *IEEE Trans. Microw. Theory Techn.*, vol. 56, no. 2, pp. 328–338, Feb. 2008.
[19] J. Kim, J. Son, J. Moon, and B. Kim, "A saturated doherty power amplifier based on saturated amplifier," *IEEE Microw. Wirel. Compon. Lett.*, vol. 20, no. 2, pp. 109–111, Feb. 2010.
[20] X. Chen, W. Chen, F. M. Ghannouchi, Z. Feng, and Y. Liu, "A broadband Doherty power amplifier based on continuous-mode technology," *IEEE Trans. Microw. Theory Techn.*, vol. 64, no. 12, pp. 4505–4517, Dec. 2016.
[21] W. Shi, S. He, X. Zhu, B. Song, Z. Zhu, G. Naah, and M. Zhang, "Broadband continuous-mode Doherty power amplifiers with noninfinity peaking impedance," *IEEE Trans. Microw. Theory Techn.*, vol. 66, no. 2, pp. 1034–1046, Feb. 2018.
[22] C. Huang, S. He, and F. You, "Design of broadband modified class-J Doherty power amplifier with specific second harmonic terminations," *IEEE Access*, vol. 6, pp. 2531–2540, 2018.
[23] M. Li, J. Pang, Y. Li, and A. Zhu, "Ultra-wideband dual-mode Doherty power amplifier using reciprocal gate bias for 5G applications," *IEEE Trans. Microw. Theory Tech.*, vol. 67, no. 10, pp. 4246–4259, Oct. 2019.
[24] A. Cidronali, S. Maddio, N. Giovannelli, and G. Collodi, "Frequency analysis and multiline implementation of compensated impedance inverter for wideband Doherty high-power amplifier design," *IEEE Trans. Microw. Theory Techn.*, vol. 64, no. 5, pp. 1359–1372, May 2016.
[25] W. Shi, S. He, F. You, H. Xie, G. Naah, Q. Liu, and Q. Li, "The influence of the output impedances of peaking power amplifier on broadband Doherty amplifiers," *IEEE Trans. Microw. Theory Techn.*, vol. 65, no. 8, pp. 3002–3013, Aug. 2017.
[26] H. Kang, H. Lee, W. Lee, H. Oh, W. Lim, H. Koo, C. Park, K. C. Hwang, K. Lee, and Y. Yang, "Octave bandwidth Doherty power amplifier using multiple resonance circuit for the peaking amplifier," *IEEE Transactions on Circuits and Systems I: Regular Papers*, pp. 1–11, 2018.
[27] P. J. Tasker and J. Benedikt, "Waveform inspired models and the harmonic balance emulator," *IEEE Microw. Mag.*, vol. 12, no. 2, pp. 38–54, April 2011.
[28] Y. Li, W. Cao, and A. Zhu, "Instantaneous sample indexed magnitude-selective affine function-based behavioral model for digital predistortion of RF power amplifiers," *IEEE Trans. Microw. Theory Techn.*, vol. 66, no. 11, pp. 5000 – 5010, Nov. 2018.
[29] J. M. Rubio, J. Fang, V. Camarchia, R. Quaglia, M. Pirola, and G. Ghione, "3–3.6-GHz wideband GaN Doherty power amplifier exploiting output compensation stages," *IEEE Trans. Microw. Theory Techn.*, vol. 60, no. 8, pp. 2543–2548, Aug. 2012.
[30] X. Fang, A. Chung, and S. Boumaiza, "Linearity-enhanced Doherty power amplifier using output combining network with predefined AM-PM characteristics," *IEEE Trans. Microw. Theory Techn.*, pp. 1–10, 2018.
[31] P. H. Pednekar, E. Berry, and T. W. Barton, "RF-input load modulated balanced amplifier with octave bandwidth," *IEEE Trans. Microw. Theory Techn.*, vol. 65, no. 12, pp. 5181–5191, Dec. 2017.
[32] J. J. M. Rubio, V. Camarchia, M. Pirola, and R. Quaglia, "Design of an 87% fractional bandwidth Doherty power amplifier supported by a simplified bandwidth estimation method," *IEEE Trans. Microw. Theory Techn.*, vol. 66, no. 3, pp. 1319–1327, Mar. 2018.

Meng Li (S'14) received the B.S. degree in Electromagnetic Field and Radio Technology and M.S. degree in Electromagnetic Field and Microwave Technology from University of Electronic Science and Technology of China (UESTC), Chengdu, China, in 2012 and 2015, respectively, and is currently working towards the Ph.D degree at University College Dublin (UCD), Dublin, Ireland.

She is currently with the RF and Microwave Research Group, UCD. Her research interests mainly focus on broadband high-efficiency power amplifiers and MMIC power amplifier design for RF/microwave and millimeter-wave applications.

Jingzhou Pang (S'13-M'16) received the B.S. degree in electrical engineering and Ph. D. degree in circuits and systems from University of Electronic Science and Technology of China (UESTC), Chengdu, China, in 2010 and 2016, respectively. In December 2016, he joined Huawei Technologies Company Ltd., Shenzhen, China, where he was a engineer in charge of the research and development of 5G high efficiency power amplifiers and transmitters. He is currently with the RF and Microwave Research Group at University College Dublin (UCD), Dubin, Ireland, as a research fellow. His research interests include broadband high-efficiency power amplifier systems, bandwidth extension techniques for high-efficiency transmitters and MMIC power amplifier design for RF/microwave and millimeter-wave applications.

Jingzhou Pang was a recipient of the EDGE Marie Sklodowska-Curie Individual Fellowship. He was a recipient of third Place Award of the High Efficiency Power Amplifier Student Design Competition, IEEE Microwave Theory and Techniques Society (IEEE MTT-S) International Microwave Symposium (IMS) in 2013.

Yue Li (S'17) received the B.E. degree in information engineering from Southeast University, Nanjing, China, in 2016. He is currently working towards the Ph.D. degree at University College Dublin, Dublin, Ireland.

He is currently with the RF and Microwave Research Group, UCD. His current research interests include behavioral modeling and digital predistortion for RF power amplifiers.

Anding Zhu (S'00-M'04-SM'12) received the Ph.D. degree in electronic engineering from University College Dublin (UCD), Dublin, Ireland, in 2004.

He is currently a Professor with the School of Electrical and Electronic Engineering, UCD. His research interests include high-frequency nonlinear system modeling and device characterization techniques, high-efficiency power amplifier design, wireless transmitter architectures, digital signal processing, and nonlinear system identification algorithms. He has published more than 130 peer-reviewed journal and conference articles.

Prof. Zhu is an elected member of MTT-S AdCom, the Chair of the Electronic Information Committee and the Vice Chair of the Publications Committee. He is also the Chair of the MTT-S Microwave High-Power Techniques Committee. He served as the Secretary of MTT-S AdCom in 2018. He was the General Chair of the 2018 IEEE MTT-S International Microwave Workshop Series on 5G Hardware and System Technologies (IMWS-5G) and a Guest Editor of the IEEE TRANSACTIONS ON MICROWAVE THEORY AND TECHNIQUES on 5G Hardware and System Technologies. He is currently an Associate Editor of the IEEE Microwave Magazine and a Track Editor of the IEEE TRANSACTIONS ON MICROWAVE THEORY AND TECHNIQUES.